Proceedings of the Canadian Society for Mechanical Engineering International Congress
32nd Annual Conference of the Computational Fluid Dynamics Society of Canada
Canadian Society of Rheology Symposium
CSME/CFDSC/CSR 2025
May 25–28, 2025, Montréal, Québec, Canada

NUMBER

Aeroacoustic analysis in a tail rotor configuration using Large Eddy Simulations and Ffowcs Williams and Hawkings' analogy

R.K POUHE HIOL[1], Marlène SANJOSÉ[1],

[1]Aerospace Engineering, École de Technologie Supérieure, Montréal, QC, Canada

***Abstract*—**Large eddy simulations (LES) are carried out in a ducted rotor configuration to extract noise sources in the unsteady turbulent flow around the blades. The latter are propagated in the far field using the Ffowcs Williams and Hawkings (FW-H) analogy and results are compared to experimental data provided by a measurement campaign in anechoic chamber. The mean flow field analysis highlights high turbulence intensity in the root of the blade and the tip gap regions where the tip leakage vortex breakdown occurs. The sensitivity of some aerodynamic coefficients to the subgrid scale model is analysed. A general improvement of sound levels, especially for broadband components, is observed compared to previous URANS simulations.

***Keywords-component*—Helicopters; Tail rotor; WMLES; WR-LES; Acoustic analogy;**

I. Introduction

The widespread use of helicopters for civil applications, has continuously increased traffic in urban areas, with a negative impact on the noise levels for surrounding populations. The stringent regulations on noise emission, enforced to protect impacted populations, are encouraging manufacturers to improve their design methods to develop quieter aircraft. To this end, the Electrically Distributed Anti-Torque (EDAT) system, a new electrically driven tail rotor design composed of four fans embedded in a shroud, has been tested and shown promising results in terms of safety, manoeuvrability and noise reduction [1]. In this context of quieter rotor design, it is important to rely on accurate aerodynamic noise prediction tools.

The various fan noise prediction methods have been categorized into three classes [2]. The first class, based on empirical models, estimates the sound power level as a function of sparse fan and operating parameters and is inappropriate for new design development. The Class II is based on the use of analytical and semi-empirical models informed by local mean flow characteristics for the noise prediction of sound distinct generating mechanisms. This approach requires a high level of modelling and may be inaccurate when exploring new design spaces. The last class is referred to as Computational Aeroacoustic (CAA), which aims to resolve the main unsteady turbulent fields that generate the far-field acoustic field. Either direct or hybrid approach can be used to compute the acoustic field in the far field [3]. In the present work, a hybrid approach which split the computation into two steps is used . First, the noise source generation in the near-field is simulated with a high-fidelity solver, and then the acoustic propagation in the far field is computed using an acoustic analogy. The aim is to obtain a better knowledge of the EDAT configuration in order to improve the noise source modelling and thus improve the reliability of Class II methods.

Previous experimental and numerical investigations have provided a comprehensive understanding of the aerodynamic and aeroacoustic characteristics of a single ducted rotor-stator system identical to those in the EDAT assembly [4, 5]. A measurement campaign in the full anechoic room at Université de Sherbrooke has provided a database of the sound generated on an arc of microphones and serves as a reference for numerical analysis. In addition, thrust, torque and rotational speed were measured on a dedicated performance test-rig for the same rotor-stator prototype. Preliminary RANS simulations allowed computing the performances of the assembly with a good agreement. Far-field noise using classical analytical approaches provide rather good estimate of tonal noise, but inaccurate broadband levels compared with experimental results. A noise mechanism decomposition analysis has shown that the rotor is the main contributor for broadband noise. Later, URANS simulations were performed and allowed a good prediction of the tones in the acoustic power spectra, but are not able to predict broadband noise levels [4], showing

poor high-frequency behaviour due to the intrinsic modelling of the turbulence.

In the present work, high fidelity simulations are carried out using large eddy simulations that resolve turbulent structures at an affordable computational cost on the rotor alone installed in the duct. These turbulent structures that developed in the flow are the main sources of broadband noise components in the far-field. Later, the noise sources are propagated in the far-field with the Ffowcs Williams & Hawkings (FW-H) equation [6], that relates the acoustic pressure $p'(\mathbf{x}, t)$ at an observer located in $\mathbf{x}$ at a time t, to the aerodynamic noise sources generated by a moving body assuming free-field propagation.

The objectives are to finely resolve the turbulence in the vicinity of the blades in order to identify the noise sources and improve the knowledge for the modelling of broadband noise sources. Such an approach, (LES + FW-H), has already been used for aeroacoustic analysis in jet noise configurations [7, 8] and successfully applied in rotor noise configurations [3, 9, 10].

The numerical methods for the LES employed in the present work are summarized in section II. Aerodynamics and aeroacoustics results obtained will be investigated in sections III and IV respectively.

II. Numerical Methods

The LES simulations are performed with **AVBP V7.9**, a compressible solver adapted to unstructured grids in turbomachinery applications [11, 12]. This section provides the main numerical parameters used in the present work.

A. Computational domain

Fig. 1 shows the computational domain employed in the LES simulations. It is composed of only the rotor part of the EDAT system, delimited to a $90°$ angular sector containing one blade of diameter D_{prop}. The green areas highlight the geometric elements that appear in the actual configuration tested experimentally. Both the hub and shroud surfaces are extruded up to the outlet, located 0.5 D_{prop} downstream of the blade. The inlet has an elliptical shape so that its local normals approximate the actual inflow directions in hover condition. The entire domain is rotated during the simulation.

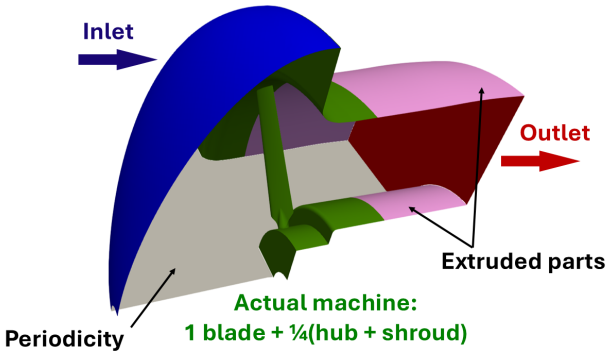

Figure. 1: Computational domain.

B. Mesh characteristics

Fig. 2 shows a meridional plane and a blade-to-blade view at 85% span of the blade. It is an unstructured hybrid grid composed of 69M tetrahedra and 10M prismatic cells. The prismatic layers have seven elements in the normal direction with a stretching ratio of 1.25 and are located around the blade surface and along the shroud to properly resolve the boundary layers.

The region downstream of the blade is refined to resolve turbulent structures in the wake of the rotor and the boundary layer developing along the shroud, as highlighted in Fig. 2a. The tip gap region is discretized radially with 14 prismatic cells (7 at each end) and about 18 tetrahedra cells in between to capture the leakage flow that will interact with the Tip Leakage Vortex (TLV). The latter is considered as a potential contributor to the far-field broadband noise. Mesh refinement is also performed for cells around the leading edge (LE) and the trailing edge (TE) of the blade, as shown in Fig. 2b. Mesh coarsening is applied towards the outlet to damp turbulent fluctuations before the outlet BC.

The mesh quality is evaluated in section III-A.

C. Numerical parameters

The simulations employ the Lax-Wendroff (LW) scheme, which is second order in time and space. The entire domain rotates at a rotational speed Ω_0 and the equations are solved in the stationary reference frame.

The Wall Adapting Local Eddy-viscosity (WALE) SGS model [13] has been used for its capabilities in the near wall regions. WALE model has been used in many turbomachinery configurations [10, 14, 15]. A comparison with other models is done in section III-D. An additional artificial viscosity [16] is used to damp non-physical oscillations introduced in the simulations by the numerical scheme or the discretisation errors. The mean time step in the computational domain is about $\Delta t_{mean} = 3.10^{-8}\ s$, constrained by a CFL of 0.7 that ensures the stability of the LW scheme.

Navier-Stokes Characteristics Boundary Conditions (NSCBC) are used for Inlet and Outlet, to avoid spurious reflection of acoustics waves at the boundaries in compressible simulations [17, 18]. The experimental mass flow rate and the reference temperature are imposed at inlet and the reference static pressure is imposed at the outlet. All solid surfaces except the shaft are set to adiabatic no-slip walls. The blade and the shroud are wall resolved, so a zero-velocity condition is applied. The logarithmic law of the wall is used to model wall-shear stress on the other wall surfaces. Periodic conditions apply in the azimuthal direction. The motion of the moving surfaces, blade and rotating hub, is taken into account by the wall boundary condition.

The convergence is obtained after 3 blade revolutions and 6 additional rotations have been simulated to record data for acoustic analysis. Flow quantities have been averaged in time over the last two revolutions and are discussed in sec. III-C.

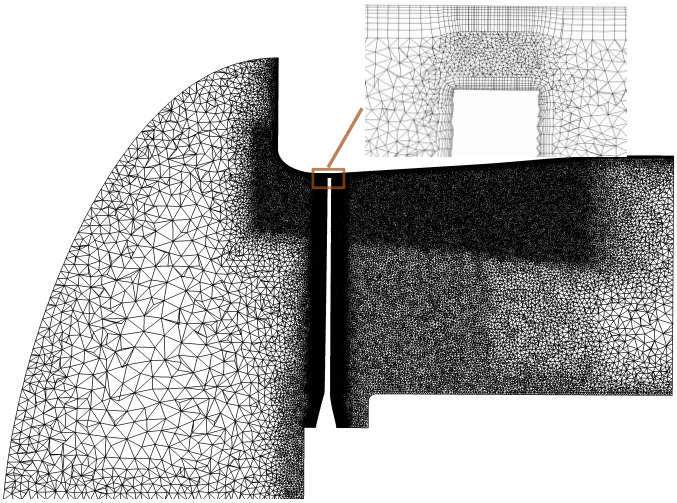

(a) Meridional plane $\theta = 0°$

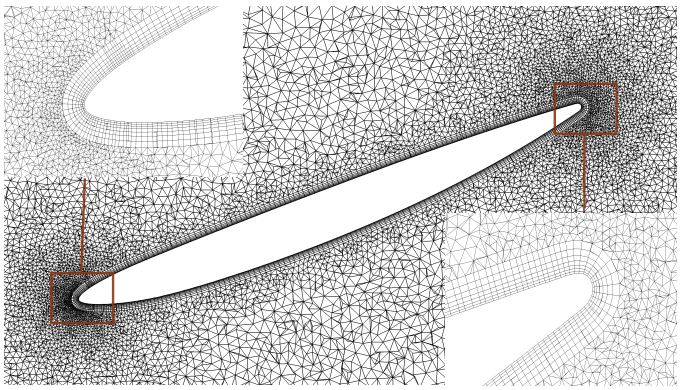

(b) Blade-to-blade cut at 85% span of the blade

Figure. 2: Mesh used for LES simulations

D. Acoustic methods

The far field noise is calculated using the FW-H analogy. The pressure field on the blade and shroud surfaces is recorded at $\Delta t_{source} = 1.5 \times 10^{-5}$ s during the simulation. The acoustic pressure is computed, using the **SherFWH** solver [19], which implements an advanced time formulation [20], on 327 microphones uniformly distributed along the longitude and latitude directions of a sphere of 1.85 m radius measured from the rotor centre. Analysis of the power spectral density (PSD) for each microphone is done using Welch's periodogram method using 7 chunks with 50% overlap, a Hanning windowing and zero padding. The acoustic spectra from the LES reach a resolution of about 30 Hz. The acoustic power (W) is obtained by integration over the sphere of microphone of the acoustic intensity $I = \frac{PSD}{Z_0}$, where $Z_0 = \rho_0 c_0$ is the air impedance. Then, the sound power levels (SWL) in dB are calculated using:

$$\mathrm{SWL} = 10 \log_{10} \left(\frac{\mathrm{W}}{\mathrm{W}_0}\right) \tag{1}$$

with $\mathrm{W}_0 = 10^{-12}\, W$, the reference sound power.

III. Aerodynamic results

Transient time has been carefully checked by looking at the convergence of integrated quantities over the domain and meridional profile of mean quantities upstream and downstream of the blade. The flow is well established after three fan revolutions. In this section mesh quality and aerodynamic performances will be investigated. Mean flow characteristics will be analysed, followed by a study of the influence of the SGS model.

A. Mesh quality

The surface mesh quality for the simulated flow can be estimated using the dimensionless wall distance y^+ obtained by the ratio between the distance of the first element from the wall and the local wall shear stress τ_w, scaled by the fluid density and kinematic viscosity.

$$y^+ = \frac{y u_\tau}{\nu}, \qquad u_\tau = \sqrt{\frac{\tau_w}{\rho}} \tag{2}$$

On the blade, an average of about 10 is found, with values around 5 in the mid-span region and local maximum in the LE and tip regions of the blade. For the shroud, the average y^+ is 6.5 with a maximal value around 28 in the tip clearance region. These values are consistent with the wall-resolved approach taken for these surfaces. The mean y^+ value on the hub is 160 with maximal value about 300 on the sharp corners. These values are also consistent for a wall-modelled approach using a log-law approach.

The volume mesh quality is assessed with the LES_IQ_v criterion developed in [21], defined as:

$$LES\_IQ_v = \frac{1}{1 + \alpha_v (\frac{<\nu_{t,eff}>}{\nu})^n}, \tag{3}$$

with $\alpha_v = 0.05$, $n = 5$, $< \nu_{t,eff} >= \nu^{SGS} + \nu$. A well resolved LES should reach the recommended values between 0.8 and 0.95 [21].

Fig. 3 shows the criterion in the meridional plane $\theta = 0°$ across the blade. The mesh fulfil the requirements in the duct section and particularly in the vicinity of the blade where the main noise sources are expected. Further downstream or upstream, the mesh coarsening, applied to damp turbulent fluctuations, is visible.

B. Performance

The thrust F_x and torque T_x produced by the rotor in the LES simulation are compared with other results obtained in previous studies. The quantities have been made dimensionless

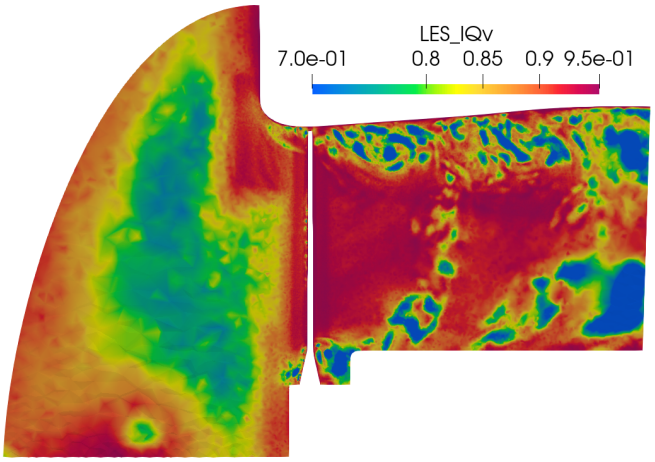

Figure. 3: LES_IQ_v criterion in the meridional plane $\theta = 0°$

in the form of the thrust C_T and torque C_Q coefficients defined as:

$$C_T = \frac{F_x}{\rho\ \Omega^2\ D_{\text{prop}}^4} \qquad C_Q = \frac{T_x}{\rho\ \Omega^2\ D_{\text{prop}}^5}. \tag{4}$$

Fig. 4 shows a comparison between LES, RANS, URANS [4], LBM [5] and experimental values of C_T and C_Q.
$\Omega^* = \frac{\Omega - \Omega_0}{\Omega_0}$ is the dimensionless rotational speed and Ω_0 the nominal rotational speed.

The surfaces that contribute to the thrust are the blades, the hub and the casing with about 70% of the thrust that come from the rotor blades. LES underestimates the thrust compared to the experimental value while the torque produced by the blades is over-predicted. These differences are mainly due to the absence of the stator whose role is to straighten the main flow in order to reduce overall aerodynamic losses caused by the tangential component of the velocity vector. The same trend can be observed with the LBM values which are quite similar to LES but very different from RANS and URANS where the contribution of the stator is included.

C. Mean Flow analysis

Figure 5 shows an isosurface of the Q-criterion, the second invariant of the velocity gradient tensor, which identifies the most coherent structures of the simulation. The TLV at the blade tip is strong and coherent for the current hover operating condition. It stays almost in the plane of rotation at an almost constant radius. The root of the blade introduces a region of strong coherent structures. The transition from laminar to turbulent regime of the boundary layer on the blade is clearly observed, and the coherent structures in the turbulent wake downstream the trailing edge. The turbulent casing boundary layer interacts with the blade tip where high turbulent pressure fluctuations are visible, but also with the TLV further downstream from the blade.

The meridional average of the turbulent kinetic energy (TKE) field is shown in Fig. 6. A zone of high turbulent structure intensity can be observed in the tip region. Another

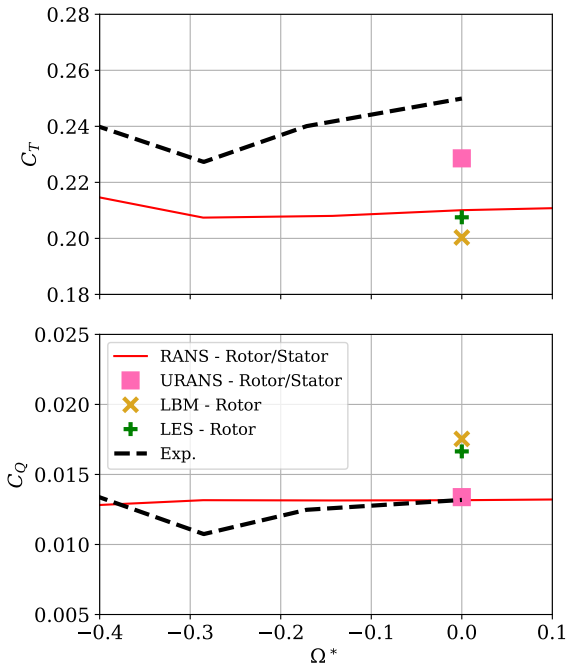

Figure. 4: Comparison of performances coefficients C_T and C_Q between LES, LBM and experimental results

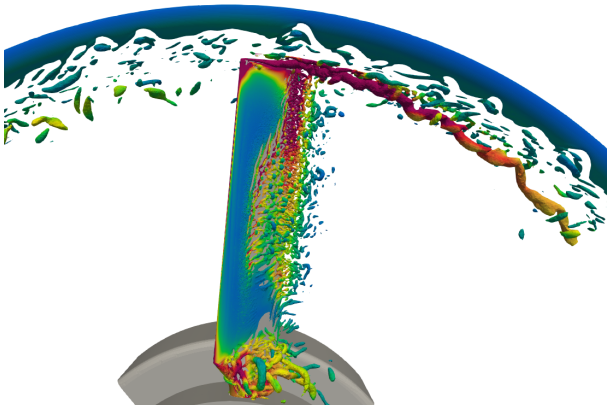

Figure. 5: Isosurface of Q-criterion of value $2 \times 10^7\ s^{-2}$ coloured by the root mean squared of the wall pressure fluctuations.

high TKE zone is observed at the inlet of the shroud, due to the flow separation that forces the transition to turbulence.

D. Influence of SGS model

This work is based on an explicit LES, where larger turbulent scales are resolved by the numerical scheme, while the effect of the smallest scales is determined by the SGS model. In order to verify the sensitivity of the performance and noise sources to the SGS models, three SGS models, Smagorinsky, WALE and Sigma, are evaluated for the present configuration. The statistics are collected for the duration of one quarter of a rotor revolution. The Smagorinsky model [22]

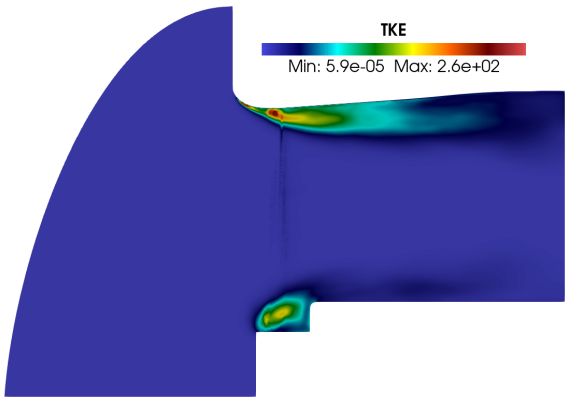

Figure. 6: Turbulence kinetic energy (TKE) field in the meridional plane

is the most commonly used in LES applications due to its ease of implementation. However, one of the drawbacks of this model is its behaviour near the walls, where the SGS viscosity decay is not fast enough. To overcome the disadvantages of the Smagorinsky model, the WALE model has been developed [13]. It is based on the square of the velocity gradient and ensures that the SGS viscosity decays correctly near walls. The Sigma model is an improvement of the WALE model based on the singular values of the velocity gradient tensor to better account for the transition [23].

Fig. 7 shows the distribution of the pressure coefficient C_p, the friction coefficient C_f and the root mean square pressure coefficient $C_{p,\mathrm{rms}}$ along the chord at different span locations for the three models. These coefficients are defined as:

$$C_p = \frac{\overline{p} - p_\infty}{\frac{1}{2}\rho W^2} \quad C_f = \frac{\overline{\tau_w}}{\frac{1}{2}\rho W^2} \quad C_{p,\mathrm{rms}} = \frac{\sqrt{\overline{p'^2}}}{\frac{1}{2}\rho W^2} \tag{5}$$

where W is the time-averaged relative velocity seen by each span section of the blade.

As expected, the Smagorinsky model provides more than 5 times larger C_f values compared to Sigma and WALE, due to the over-estimation of the SGS viscosity at the wall. This modifies the mean C_p distribution but also changes the $C_{p,\mathrm{rms}}$ distribution drastically, hence the noise sources. WALE and Sigma C_p and C_f curves have the same shapes with very minor differences. In the C_p plots, a plateau can be associated with a laminar separation bubble. This is the case at 40% chord and 85% chord at mid-span and upper span blade sections respectively. Larger differences between WALE and Sigma can be noticed in the $C_{p,\mathrm{rms}}$ values, but the two distributions are very similar. In particular, the transition is captured at the same location along the chord and maximum pressure fluctuations have very similar levels. These results highlight the significant impact of the SGS model in the near wall regions of wall bounded flows with Wall Resolved LES (WRLES) compared to those presented in [24] where no major variations were observed on the static pressure across the blade when a wall law is used. The change in mean C_p distribution with the Smagorinsky model has high effects on the values of performance coefficients as shown in Tab. I. Sigma model shows very little improvement to WALE results with a relative higher computational cost due to the eigenvalue problem to be solved. For this reason, the WALE model has been used in the results of the following sections.

TABLE. I: C_T and C_Q for the three SGS models

	Smagorinsky	Sigma	WALE
C_T	0.149	0.212	0.212
C_Q	0.0143	0.0167	0.0168

IV. Aeroacoustic Results

This section presents qualitative and quantitative analysis of the acoustic field resolved with this configuration.

Fig. 8a and Fig. 8b show the divergence of the field to identify the acoustic wavefronts in a meridional plane and a blade-to-blade plane at 95% of the blade span. The noise sources are clearly emitted from the upper part of the blade. The blade-to-blade view near the tip shows radially propagating waves from the trailing edge, with phase shift between blade sides characteristic of a dipolar noise emission. Noise reflections on the casing may explain the lower and flatter wave patterns travelling back from the downstream side.

The acoustic power (SWL) is plotted in Fig. 9 and compared to experiments and previous URANS simulations. The scale of the vertical axis is 20 dB between two graduations. The kink observed at high frequencies in the experiments curve is likely due to installation effects [5]. The peaks at the blade passing frequency (BPF) and its harmonics are captured as well as the secondary peaks around the BPF but with smaller amplitude compared to experiments, given the limited resolution frequency of 30 Hz reached in the LES spectra. The first two harmonics were not captured with the URANS simulations. In addition, the LES simulations provide an excellent broadband noise shape. However, the broadband levels are still overpredicted by 5-10 dB.

V. Conclusion

High fidelity simulations using Large Eddy Simulation (LES) were carried out of the flow in a single fan that comprised the Electrically Distributed Anti Torque system concept for hovering conditions. The aerodynamic performance coefficients obtained without the stator vanes are consistent with measurements made on the actual rotor-stator assembly. The flow analysis has provided significant information for the noise source analysis. In particular, the flow is strongly influenced by transition effects along the blade span, but also on the casing walls. The far field acoustic power calculated using the FW-H analogy results has confirmed that the rotor is the main noise contributor. The LES results outperform both the tonal and broadband sound level predictions compared to URANS. The study of the influence of the SGS model has highlighted its influence on the blade loading, and even more its influence on the resolved turbulent fluctuations. The Smagorinsky model was unable to capture the transition and underpredicted the performance coefficients, confirming its limitations in wall

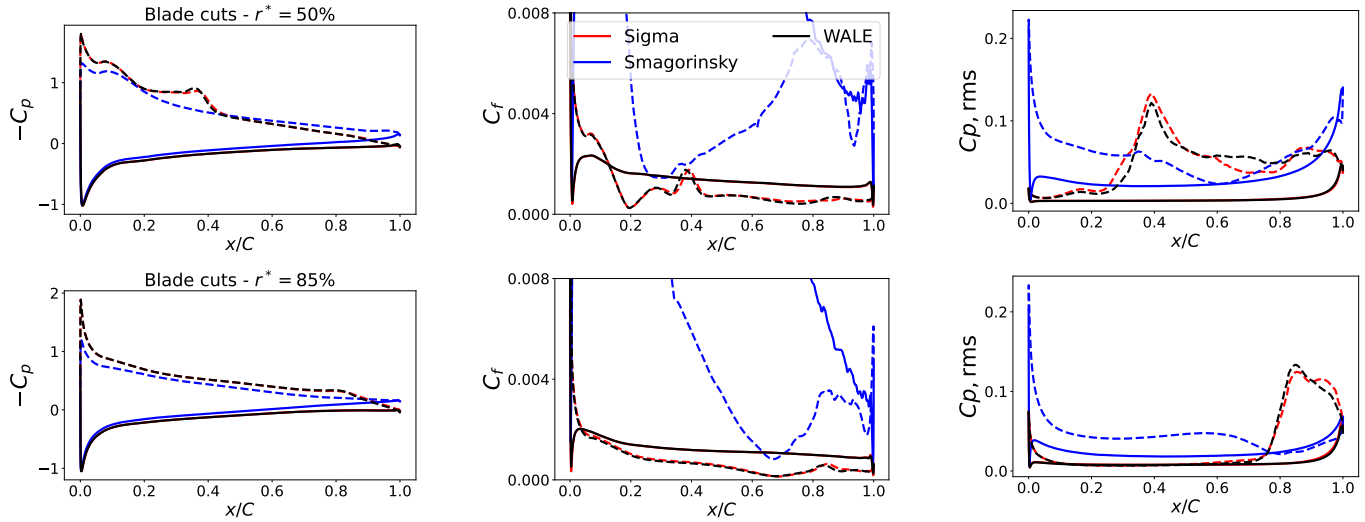

Figure. 7: Comparison of C_p, C_f and $C_{p,\mathrm{rms}}$ at 50% and 85% of the span for Smagorinsky (blue), WALE (black) and Sigma (red) models. Continuous lines: pressure side, dashed lines: suction side.

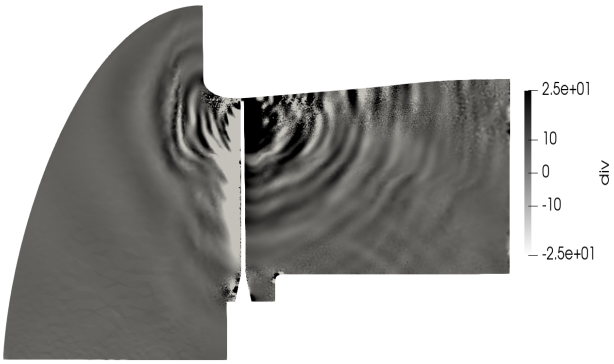

(a) Meridional plane $\theta = 0°$

(b) Blade-to-blade cut at 95% of span

Figure. 8: Dilatation field in (a) the meridional plane $\theta = 0°$ and (b) the blade-to-blade cut at 95% of the span.

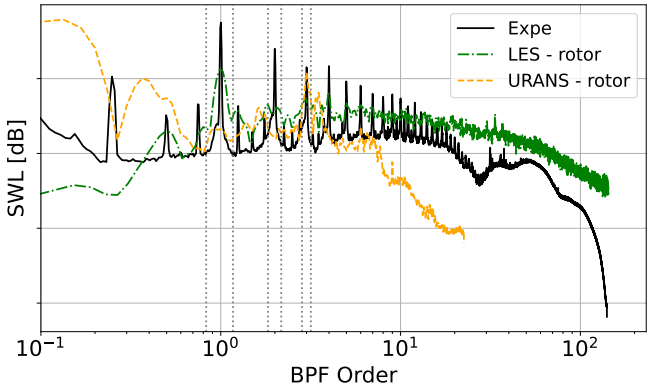

Figure. 9: Sound Power Levels (SWL) generated at a sphere of microphones located at 1.85m of the rotor

bounded flows with the WRLES approach at this Reynolds number. Further work should also consider the use of a less dispersive and dissipative numerical scheme. These simulations provide an accurate database for the development of models of the wall pressure fluctuation spectra.

ACKNOWLEDGMENT

This work was conducted as part of research project ALLRP-570863-21 funded by NSERC and Mitacs with contributions from Optis Consultants Inc. and Bell Textron Canada Limited. The simulations and their analysis were performed on the Niagara supercomputer operated by SciNet and managed by the Digital Research Alliance of Canada. The authors want to thank the Centre Européen de Recherche et de Formation Avancée en Calcul Scientifique (CERFACS), which develops and provides us with AVBP for academic research. Post-processing was enabled in part by means of the Antares Python API developed by CERFACS.

REFERENCES

[1] B. Perry, "Program update: Bell's EDAT electric tail rotor system," May 2021.

[2] T. Carolus, *Fans: Aerodynamic Design - Noise Reduction - Optimization*. Wiesbaden, Germany [Heidelberg]: Springer Vieweg, 2022.

[3] S. Moreau, "The third golden age of aeroacoustics," *Physics of Fluids*, vol. 34, p. 031301, Mar. 2022.

[4] M. Sanjosé, "Interaction noise for a rotor-stator assembly in a short duct." https://doi.org/10.5281/zenodo.14041738, Oct. 2023.

[5] J. Rendon, P. Jaiswal, M. Sanjosé, Y. Pasco, and S. Moreau, "Aeroacoustic investigation of a ducted tail rotor using the lattice-boltzmann method," p. ID 82, 2023.

[6] JE. Ffowcs Williams and DL. Hawkings, "Sound generated by turbulence and surfaces in arbitrary Motion," *TR Soc. A*, vol. 264, pp. 21–342, 1969.

[7] A. S. Lyrintzis and M. Coderoni, "Overview of the Use of Large-Eddy Simulations in Jet Aeroacoustics," *AIAA Journal*, vol. 58, pp. 1620–1638, Apr. 2020.

[8] M. A. Alhawwary and Z. J. Wang, "Implementation of a FWH approach in a high-order LES tool for aeroacoustic noise predictions," in *AIAA Scitech 2020 Forum*, (Orlando, FL), American Institute of Aeronautics and Astronautics, Jan. 2020.

[9] D. Lewis, S. Moreau, M. C. Jacob, and M. Sanjosé, "ACAT1 Fan Stage Broadband Noise Prediction Using Large-Eddy Simulation and Analytical Models," 2022.

[10] T. Leonard, M. Sanjose, S. Moreau, and F. Duchaine, "Large Eddy Simulation of a scale-model turbofan for fan noise source diagnostic," in *22nd AIAA/CEAS Aeroacoustics Conference*, (Lyon, France), American Institute of Aeronautics and Astronautics, May 2016.

[11] T. Schönfeld and M. Rudgyard, "Steady and Unsteady Flow Simulations Using the Hybrid Flow Solver AVBP," *AIAA Journal*, vol. 37, pp. 1378–1385, Nov. 1999.

[12] N. Gourdain, F. Sicot, F. Duchaine, and L. Gicquel, "Large eddy simulation of flows in industrial compressors: A path from 2015 to 2035," *Philosophical Transactions of the Royal Society A: Mathematical, Physical and Engineering Sciences*, vol. 372, p. 20130323, Aug. 2014.

[13] F. Nicoud and F. Ducros, "Subgrid-Scale Stress Modelling Based on the Square of the Velocity Gradient Tensor," *Flow, Turbulence and Combustion*, vol. 62, pp. 183–200, Sept. 1999.

[14] G. Medic, "Application of large-eddy simulation to turbomachinery components in aircraft gas turbine engines," in *10th International ERCOFTAC Symposium on Engineering Turbulence Modeling and Measurements*, 2014.

[15] D. Papadogiannis, F. Duchaine, F. Sicot, L. Gicquel, G. Wang, and S. Moreau, "Large eddy simulation of a high pressure turbine stage: Effects of sub-grid scale modeling and mesh resolution," in *Turbo Expo: Power for Land, Sea, and Air*, vol. 45615, p. V02BT39A018, American Society of Mechanical Engineers, 2014.

[16] A. Jameson, W. Schmidt, and E. Turkel, "Numerical solution of the Euler equations by finite volume methods using Runge Kutta time stepping schemes," in *14th Fluid and Plasma Dynamics Conference*, (Palo Alto,CA,U.S.A.), American Institute of Aeronautics and Astronautics, June 1981.

[17] T. J. Poinsot and SK. Lelef, "Boundary conditions for direct simulations of compressible viscous flows," *Journal of computational physics*, vol. 101, no. 1, pp. 104–129, 1992.

[18] C. S. Yoo, Y. Wang, A. Trouvé, and H. G. Im, "Characteristic boundary conditions for direct simulations of turbulent counterflow flames," *Combustion Theory and Modelling*, vol. 9, pp. 617–646, Nov. 2005.

[19] A. Fosso Pouangué, M. Sanjosé, S. Moreau, G. Daviller, and H. Deniau, "Subsonic Jet Noise Simulations Using Both Structured and Unstructured Grids," *AIAA Journal*, vol. 53, pp. 55–69, Dec. 2014.

[20] D. Casalino, "An advanced time approach for acoustic analogy predictions," *Journal of Sound and Vibration*, vol. 261, no. 4, pp. 583–612, 2003.

[21] IB. Celik, ZN. Cehreli, and I. Yavuz, "Index of resolution quality for large eddy simulations," 2005.

[22] J. Smagorinsky, "GENERAL CIRCULATION EXPERIMENTS WITH THE PRIMITIVE EQUATIONS: I. THE BASIC EXPERIMENT*," *Monthly Weather Review*, vol. 91, pp. 99–164, Mar. 1963.

[23] F. Nicoud, H. B. Toda, O. Cabrit, S. Bose, and J. Lee, "Using singular values to build a subgrid-scale model for large eddy simulations," *Physics of Fluids*, vol. 23, p. 085106, Aug. 2011.

[24] D. Papadogiannis, F. Duchaine, L. Gicquel, G. Wang, and S. Moreau, "Effects of Subgrid Scale Modeling on the Deterministic and Stochastic Turbulent Energetic Distribution in Large-Eddy Simulations of a High-Pressure Turbine Stage," *Journal of Turbomachinery*, vol. 138, p. 091005, Sept. 2016.